Chemical Engineering Journal 534 (2026) 174960

Contents lists available at ScienceDirect

Chemical Engineering Journal

journal homepage: www.elsevier.com/locate/cej

Digitalization of microbial electrosynthesis: Understanding operational variables for ethanol production optimization

Jorge A. Albarracin-Arias [a], Meritxell Romans-Casas [a], Paolo Dessì [b], M. Dolors Balaguer [a], Sebastià Puig [a,*]

[a] LEQUiA, Institute of the Environment, University of Girona. Campus Montilivi, Carrer Maria Aurèlia Capmany 69, E-17003, Girona, Spain
[b] Department of Agricultural Sciences, University of Naples Federico II, Piazza Carlo di Borbone 1, 80055, Portici, Italy

ARTICLE INFO

Keywords:
Biofuels
CO_2 bio-electrorecycling
Process data mining
Ethanol selectivity
Multiple-phase analysis

ABSTRACT

Microbial electrosynthesis (MES) is a bioelectrochemical technology devoted to carbon dioxide (CO_2) conversion into value-added organic products. Traditionally, it has been addressed through trial-and-error approaches, with limited experimental data. This study introduces a data-driven framework to advance the MES digitalization through systematic analysis of operational variables influencing CO_2 conversion. CO_2 conversion to acetic acid and ethanol was investigated in MES cells integrated within an automated bench-scale platform. It enabled real-time control of key operational variables, i.e. dissolved CO_2, pH, and pressure, while monitoring electrical conductivity, cell voltage and temperature. The ethanol production rate was improved by 35% (14.80 g $m^{-2}d^{-1}$), obtained controlling dissolved CO_2 at 100–300 mg L^{-1}, pH at 4.5–4.8 and pressure at 1.8 bar. Process data were analyzed through pattern discovery (based on both operation and production variables) and unsupervised clustering (based solely on operational variables). The latter allowed to identify distinct operational phases, which matched the real production stages, solely based on operation variables. Principal component analysis revealed that acetic acid production was primarily dependent on dissolved CO_2, with secondary contributions from pH and electrical conductivity. Electrical conductivity emerged as an identifying signal for ethanol production. The proposed data-based methodology elucidates the key variable interactions and supports phase-specific monitoring and control strategies for MES optimization in the absence of time-consuming, punctual product measurements.

1. Introduction

Microbial electrosynthesis (MES) has emerged as potential route for carbon dioxide (CO_2) recycling into value added compounds [1]. Through MES, CO_2 can be converted into valuable compounds such as methane, volatile fatty acids (VFAs) and alcohols [2]. Although acetic acid (HA) and methane have been the most common products obtained through MES, their low market value (0.58 and 0.11 EUR kg^{-1}, respectively) [3] hampers economic feasibility [4]. Therefore, MES development could focus on a higher value product like ethanol (EtOH) (1.01 EUR kg^{-1}) [5], which is gaining increasing market relevance as drop-in biofuel for transportation decarbonization. EtOH can also serve as electron donor for the bio-based production of valuable medium chain carboxylates [6,7].

EtOH production in MES is usually carried out by acetogenic bacteria that in a first stage reduce CO_2 to HA through the Wood Ljungdahl Pathway (WLP) [8]. Upon HA accumulation and pH decrease near its pK_a (4.75), the same bacteria activate a detoxifying mechanism where HA is reassimilated and converted to EtOH [8]. EtOH production (solventogenesis) from HA was demonstrated in fermentation bottles by Steinbusch et al. [9], applying slightly acidic pH (5) and H_2 overpressure to boost the reaction thermodynamics. Later, in bioelectrochemical systems, CO_2 reduction to HA and EtOH in cathodes was addressed through different strategies. For instance, double-chamber microbial electrosynthesis cell equipped with gas diffusion electrode (GDE), continuously fed with CO_2 (15 mL min^{-1}) resulted in an EtOH production of 8.46 g m^{-2} d^{-1} by an enriched mixed culture [10]. The same study revealed that solventogenesis was activated when pH decreased below 4.5 and the total inorganic carbon was between 300 and 600 mg L^{-1}. As CO_2 concentration and pH are critical to trigger solventogenesis,

* Corresponding author.
E-mail addresses: jorgealberto.albarracin@udg.edu (J.A. Albarracin-Arias), meritxell.romans@udg.edu (M. Romans-Casas), paolo.dessi@unina.it (P. Dessì), dolors.balaguer@udg.edu (M.D. Balaguer), sebastia.puig@udg.edu (S. Puig).

https://doi.org/10.1016/j.cej.2026.174960
Received 14 November 2025; Received in revised form 10 February 2026; Accepted 5 March 2026
Available online 6 March 2026

Blasco-Gómez et al. [11] studied a tubular MES reactor and proposed low dissolved CO_2 (dCO_2 < 100 mg L^{-1}) and pH (<5.4) to promote solventogenesis upon HA accumulation. Later, Romas-Casas et al. [12] achieved an EtOH production rate of 10.95 g m^{-2} d^{-1} using an H-type reactor capable of withstanding high pressure (up to 3.0 atm) after HA accumulation to 6 g L^{-1}, showing that also P_{H2} has a crucial role in triggering solventogenesis.

Despite MES showing great potential for EtOH production, further process optimization is needed to achieve industrial-scale adoption. A key challenge lies in understanding how multiple interdependent operational variables influence EtOH productivity and selectivity. Data-rich experimentation therefore offers a powerful mean to develop systematic process knowledge and guide MES optimization. Romans-Casas et al. [13] operated an automated bench scale MES platform with online monitoring and precise control of the key operational variables, obtaining substantially higher production rates (5.69 g m^{-2} d^{-1}) than in a stand-alone system (1.24 g m^{-2} d^{-1}). Such an improvement was attributed to the crucial role of the joint, in-line control of key operational conditions. In details, after HA was accumulated at the cathode, pH was set in the range from 4.5 to 4.7, and dCO_2 between 200 and 800 mg L^{-1} to promote solventogenesis [13]. Such studies represent the first steps towards the digitalization of MES.

CO_2 conversion in MES is inherently dynamic, with distinct operational phases (acetogenesis and solventogenesis), each governed by specific physicochemical conditions [14]. Real-time monitoring provides an opportunity to segment and interpret these stages through data-driven analysis, revealing the operational transition that dictate EtOH formation.

Data-intensive experimentation supported by automated platforms, and data mining approaches provides a novel opportunity to understand the process and could be implemented to extract insights from the process data. In manual expert analysis, time-sequenced operational data can uncover patterns that are valuable for process optimization. However, when large and rapidly generated process datasets are involved, unsupervised methods like clustering algorithms facilitate a swift understanding of process dynamics. Unsupervised clustering aims to divide data into groups in which every observation in a cluster is internally similar to each other, but different from the observations in the other clusters [15]. While data-driven methodologies have been successfully applied in established biotechnological processes such as cell culture and wine fermentation [16,17], their application to MES remains largely unexplored. To date, most data-based methods in bio-electrochemical systems have focused on microbial fuel cells (MFCs) or microbial electrolysis cells (MECs) [18,19], leaving a critical gap in MES research. To the best of the author's knowledge, this is the first study proposing data-based analytical methods to optimize and digitalize MES.

This study aims to optimize and intensify EtOH production in MES by combining experimental tests to data-based approaches such as pattern discovery and unsupervised clustering. This provides a data-driven framework to interpret CO_2 bio-electrorecycling dynamics, identifying the most relevant operational variables for achieving high-rate and selective EtOH production in MES.

2. Materials and methods

2.1. MES platform set up

Two flat-plate MES cell stacks (Electro MP Cell, ElectroCell Europe, Denmark), named R-A and R-B, were assembled and operated in an automated plant (Fig. 1). Each reactor consisted of four cathode and four anode chambers. The cathode electrodes consisted of four carbon felts in contact with three stainless steel plates working as current collectors. The total working area of the four cathode electrodes was 0.04 m^2. The anode electrode consisted of two plates (four active faces) of dimensionally stable anode (DSA—O_2) with a total projected area of 0.04 m^2. Cathode and anode chambers were separated by cation exchange membranes (CEM, Nafion N424, USA). Both cathode and anode compartments held a total volume of 0.3 L. The electrodes were connected to a power source (MQR120-24F; Mibbo, China) in a two-electrode configuration.

Two pipeline circuits were responsible for recirculating catholyte and anolyte through the MES cells. The cathode circuit consisted of a catholyte buffer tank (1.5 L) and a micro-pump (GJ-N27-DELEE, MicroPump, USA) delivering the catholyte from the buffer tank to a probe holder containing the monitoring sensors. The catholyte was then introduced to the MES cell in an up-flow mode and parallelly for each cathode chamber, ensuring continuous contact between the liquid phase

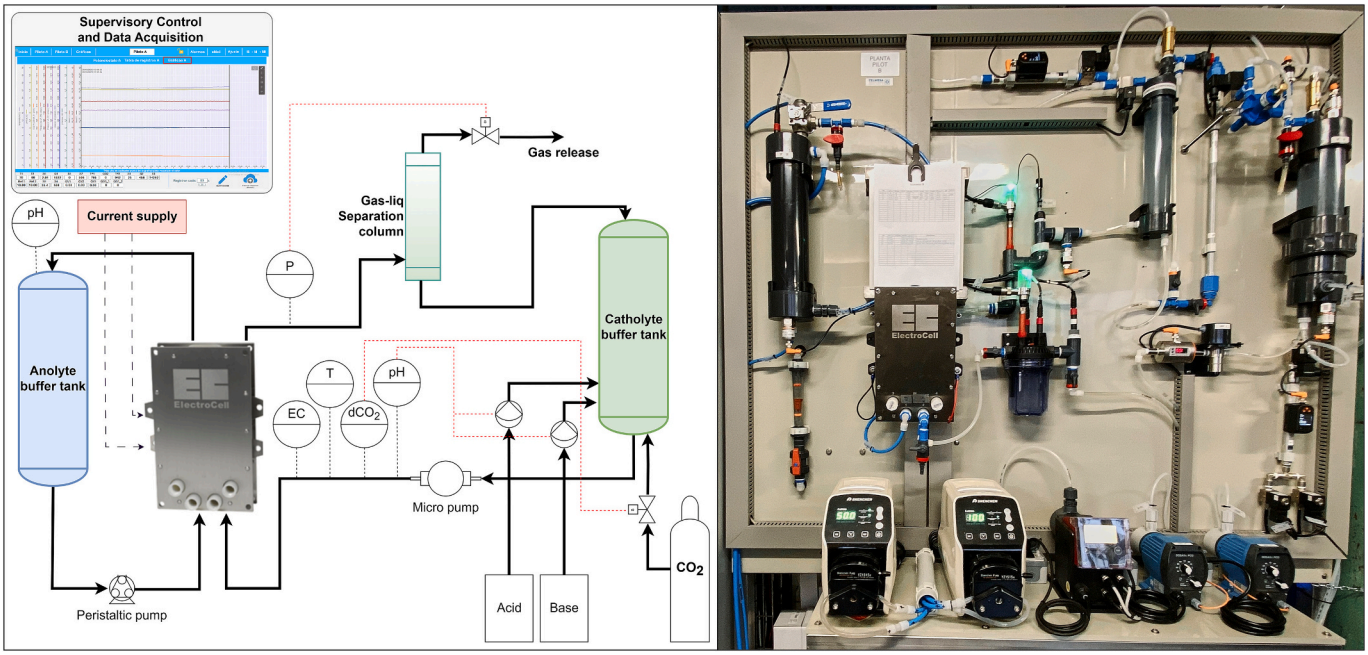

Fig. 1. Schematic overview and picture of the bench scale MES platform.

and the carbon felt electrode surface. Then, the catholyte output reached a gas-liquid separation column where non dissolved gases are separated. The liquid fraction of the separation column was returned to the buffer tank and recycled continuously. The buffer tank had input connections with a synthetic CO_2 gas cylinder (99.9%, AirLiquide, Spain) for substrate supply, and two streams of HCl and NaOH 5 M for pH control. The anode circuit consisted of a buffer tank (1.5 L) and a peristaltic pump (LabM6, Schenchen, China) that fed the anolyte parallelly to the four anode chambers of MES cells in concurrent with the catholyte. The anolyte outlet was directly recirculated to the buffer tank.

The automated plant measured dissolved CO_2 concentration (dCO_2), electrical conductivity (EC), pressure (P), and temperature (T) in the catholyte, while pH was measured in both the catholyte and anolyte streams. dCO_2 was measured before entering the MES cells using a sensor InPro® 5000(i) (Mettler Toledo, Spain) and controlled by an electro-valve (Solenoide NC, Regaber, Spain) that allowed CO_2 sparging to the catholyte in the buffer tank. The catholyte pH control was based on the pH measurement (easySense pH 32, Mettler Toledo, Spain) and dosing pumps (DOSATec PCO, Dosatronic, Spain) delivering HCl 5 M or NaOH 5 M to the buffer tank when required. P in the catholyte circuit was measured with a pressure transducer (PT0505, IFM, Spain) at the reactor outlet and controlled in the gas-liquid separation column via a gas relief electro-valve (Solenoide NC, Regaber, Spain). All process operational signals were transmitted to a programmable logic controller (PLC – H02W, Haiwell, China) which implemented the control strategies described in Table 1. The automated plant included a supervisory control and data acquisition (SCADA) system displaying the operational variables in real time and enabling the configuration of control conditions for each experiment.

2.2. Systems start up and operation

The MES stacks (R-A and R-B) were loaded with fresh electrolyte, 2.7 L for the catholyte and 2 L for the anolyte. The electrolyte consisted of a modified ATCC 1754 mineral media, prepared according to Romans-Casas et al. [12]. Electrolytes were loaded to the reactor by the hydraulic circuits providing continuous recirculation through the cathode and anode chambers.

The R-A cathode was inoculated with 0.3 L (10% v/v) of catholyte from a previously operated EtOH producing MES cell [12]. The inoculum employed hold an enriched community of >80% of *Clostridium autoethanogenum/Clostridium ljungdahlii* that reported EtOH production capability. As R-B was started up later, it was inoculated with 0.15 L of the same inoculum used for R-A inoculation plus 0.15 L of catholyte from R-A. Thus, the total catholyte working volume was 3 L.

The MES stacks were operated under galvanostatic regime at a constant applied current of 11.25 A m^{-2} while the cell voltage (E_{cell}) was monitored throughout the experiment. The only carbon source was CO_2, fed periodically according to the set range shown in Table 1. The MES stacks were operated under different conditions aiming to achieve the highest EtOH production rates. Cathode pH, dCO_2 and P were controlled on-line, according to the set values summarized in Table 1. Both reactors were operated at room temperature (15.6–31.3 °C).

Both reactors were operated in batch mode following an acetogenesis-to-solventogenesis strategy. A first operational period was oriented to produce and accumulate HA (days 0–30 for R-A, and days 0–27 for R-B). The MES stacks controllers were set to maintain high dCO_2 (1000–1250 mg L^{-1}), and pH in the range 4.8–5.0, according to previous studies [11,20]. Afterwards, the conditions were switched to promote HA reduction to EtOH. In R-A, different ranges of dCO_2 pH and P were tested (Table 1) aiming to find the optimal combination for EtOH production. Each condition was maintained until reaching a stable EtOH production (for a minimum duration of 15 days). In R-B the best conditions for EtOH production as identified in R-A (dCO_2 = 100–300 mg L^{-1}, pH = 4.5–4.8, and P = 1.8 bar) were implemented after the HA production stage.

2.3. Chemical analysis and calculations

Catholyte, anolyte and cathode gas samples were collected 2–3 times per week to confirm the accuracy of the in-line operational variables and to quantify the products. The withdrawn liquid volume was replaced with fresh media. Liquid samples were analysed for optical density at 600 nm, pH (Sension+ PH3, Hach, USA) and EC (Sension+ EC7, Hach, USA). Subsequently, samples were filtered using 0.2 μm pore filter (GSWP04700, Agilent, USA) to determine carboxylic acids and alcohols concentration by Gas Chromatography (GC). The GC instrument (7890 A GC, Agilent technologies, USA) was equipped with a polar capillary column (DB-FFAP) and a flame ionization detector (FID).

Gas samples were collected from the headspace of the liquid-gas separation column in a 5 mL gas tight syringe (Hamilton, USA). Gas composition (CO_2, H_2, CO, CH_4, O_2, and N_2) was analysed by gas chromatography (490 Micro GC system, Agilent technologies, USA), following the same instrument conditions applied by Rovira-Alsina et al. [20].

The product selectivity (%) was calculated as the percentage of the amount (mg C) of compound *i* produced to the total amount (mg C) of all organic products formed in the same timespan (Eq. 1).

$$Sel = \frac{\Delta m_i}{\sum_{j=1}^{n} \Delta m_j} \times 100 \quad (1)$$

Production rates (g m^{-2} d^{-1}) were calculated according to Eq. 2. Where ΔC_i is the product concentration (g L^{-1}) between sampling events Δt (d), and A_s is the area of electrode per volume of liquid (m^2 L^{-1}).

$$Production\ Rate = \frac{\Delta C_i}{A_s{}^{*}\Delta t} \quad (2)$$

2.4. Process data mining

Continuous data from dCO_2, pH, EC, T and E_{cell} (from now on, operational variables: O.V.) were collected with a frequency of one minute. This data, together with the samples analysis taken 2–3 times per week, were used to gain knowledge on the process with two different approaches (Fig. 2). The first data-based approach (i) consisted of pattern discovery during selected production stages based on organics concentrations (from now on, production variables: P.V.). The second strategy (ii) consisted of unsupervised clustering based only on O.V.

The pattern discovery analysis was carried out at the end of MES cells operation (231 days and 111 days for R-A and R-B, respectively). Each experimental run was divided into “stages”, defined as the periods where the process presented a stable HA and/or EtOH production trend (P.V.). For each stage, the respective O.V. dataset was analysed. O.V.

Table 1
Set conditions for controlled variables in MES reactors.

	Reactor A						Reactor B	
Operational period (days)	0–30	30–63	63–86	86–147	147–172	172–231	0–27	27–111
dCO_2 (mg L^{-1})	1000–1250	200–800		100–300	100–150	100–300	1000–1250	100–300
pH	4.8–5.0	4.5–4.8					4.8–5.0	4.5–4.8
Pressure (bar)	1.6		1.8				1.6	1.8

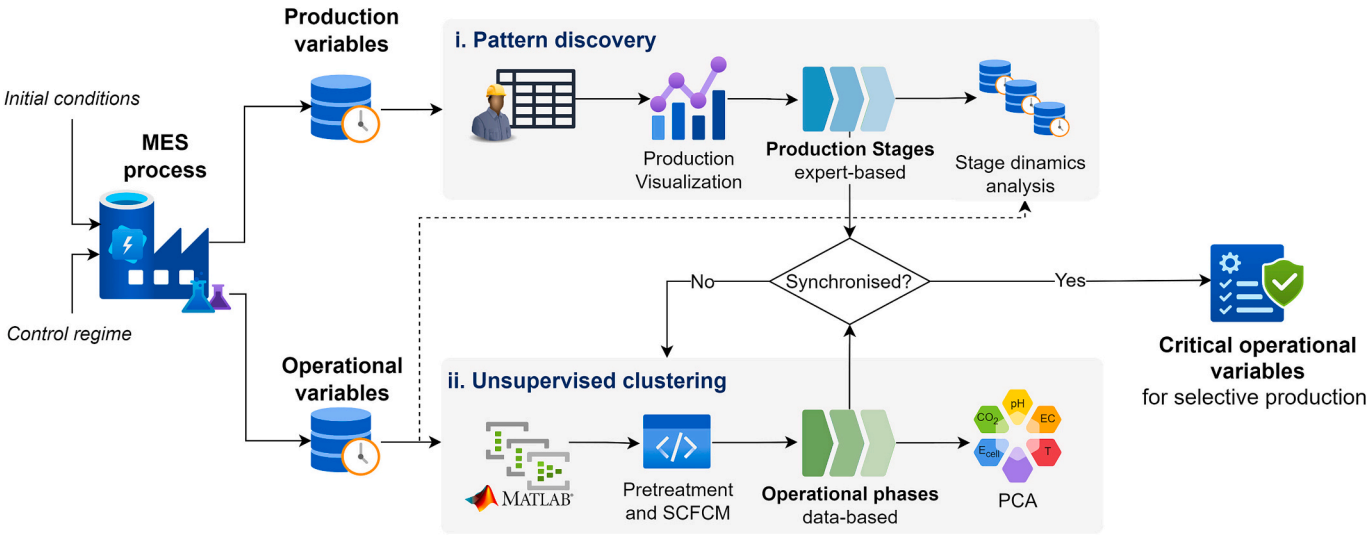

Fig. 2. Methodology used to mine time-sequenced MES process data. Production data allows to divide batch in stages while operational data was processed by Sequence Constrained Fuzzy C Means (SCFCM) to identify phases. Stage dynamic analysis was carried out for pattern discovery, while Principal Component Analysis (PCA) was carried out to find critical variables in each operational phase. When phases and stages were synchronized, production was correlated to operational conditions.

data pretreatment was applied as follow; samples were retimed to 5 min frequency using the mean value, missing values were imputed by linear interpolation, outliers were identified using a moving median–based approach with a 5 h sliding window and a threshold of 3.5 times the median absolute deviation. Detected outliers were replaced by linear interpolation. Qualitative visual analysis was based on the time-series plot, while quantitative analysis was based on the local slopes of variable signals ($\Delta variable\ \Delta t^{-1}$). The dynamics (slopes) associations among O.V. were extracted using the Slope Analyzer tool and statistically evaluated throughout the Spearman rank correlation coefficient (r') method available in OriginPro [21]. The Spearman rank correlation coefficient was selected because the operational variable dynamics were not normally distributed and their relationships were non-linear.

For the unsupervised operational clustering, only the O.V. datasets from the entire experimental run were considered. After pretreatment, all variables were resampled to 1 h frequency applying the mean value and standardized using the z-score method [15]. Phase identification was performed by partitioning the O.V. datasets using the Sequence-Constrained Fuzzy C-Means (SCFCM) algorithm, as described by Luo et al. [22]. The SCFCM algorithm divides the sequential data $X = \{x_1, x_2, \ldots, x_n\}$ of n observations into c clusters, referred to as "phases". The algorithm applied used a fuzziness coefficient of $s = 2$ and the Euclidean distance metric. Cluster memberships were initialized through cumulative temporal-distance segmentation to preserve phase continuity. The objective function minimized (heterogeneity) is defined as Eq. 3:

$$L = \sum_{i=1}^{c} \sum_{j=1}^{n} u_{ij}^{s} \left|\left|x_j - c_i\right|\right|^2 \tag{3}$$

Where u_{ij} is the membership degree of sample j to cluster i, x_j is the data vector, and c_i is the cluster center. Temporal continuity was enforced by restricting membership updates to adjacent clusters. Convergence was reached when no further reduction in the global heterogeneity L was achieved. Data samples were assigned to each phase when the corresponding membership degree exceeded 0.9.

The optimal number of clusters was selected by minimizing the Partition Performance Combination Index (PPCI), evaluated for 1–10 clusters, in Eq. 4.

$$PPCI_c = \gamma \widehat{L}_c + (1+\gamma)\widehat{c} \tag{4}$$

Where $\widehat{L}_c$ and $\widehat{c}$ are the normalized logarithm of the heterogeneity and the normalized number of clusters, respectively. γ is a weighting factor and equal to 0.6. PPCI enables the identification of the optimal number of phases by minimizing the sum-of-squares-error (SSE), while ensuring the quality of the partitioning with low computational complexity [23].

After partition, phases datasets were submitted to Principal Component Analysis (PCA) to understand which one of the operational variables provides the most variance to the system in each phase by reporting the loading plots of the two principal components. Data pretreatment, SCFCM algorithm and PCA were performed in software Matlab [24]. PCA is a multivariate statistical method applied to batch processes to evaluate strategies to monitor and diagnose faults through process data [25]. PCA aims to obtain fewer new variables (Principal Components) constituted as a linear combination of the original operational variables (O.V.). Ordered by significance, these principal components explain the largest sources of variation in the data [25,26].

Finally, time limits obtained from stage selection are compared to those obtained through phase identification with the unsupervised clustering. In case time limits of phases are synchronized with stages, it can be said that O.V. dynamics were associated to a determined production scenario either towards HA, EtOH or both simultaneously produced. This information provides a statistical model based on O.V. that governs production without inputting actual P.V. Therefore, the model will elucidate the critical variables needed to maintain the process under such state.

3. Results and discussion

3.1. Microbial electrosynthesis process evolution

MES cells were initially operated with high CO_2 availability aiming at promoting HA formation. Thus, key operation conditions in R-A were set at dCO_2 = 1000–1250 mg L^{-1}, pH = 4.8–5.0 and P = 1.6 bar (Table 1). HA was first detected on day 6 and reached a highest concentration of 90.6 mM C on day 30 (Fig. 3), indicating successfully adaptation of the inoculum to the bench-scale platform conditions. Upon HA accumulation, from day 30 onwards, the operational conditions were switched to trigger solventogenesis.

In details, dCO_2 was set between 100 and 800 mg L^{-1}, pH range was lowered to 4.5–4.8, and pressure maintained at a maximum of 1.6–1.8

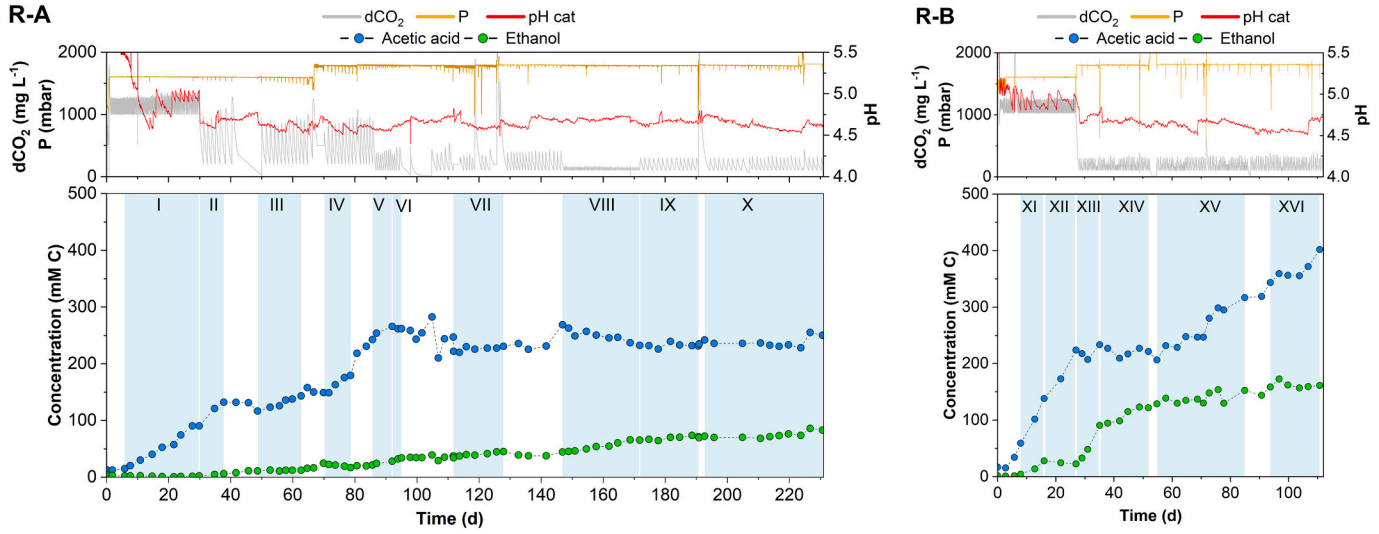

Fig. 3. Operational variable signals (dCO_2, pH in catholyte and OP) and organics (acetic acid and ethanol) concentration over time for Reactor A and B. Blue periods are the selected production stages.

bar to promote solventogenesis, according to the conditions described in Table 1. This was based on previous reports [11,12], stating that low CO_2 availability and the corresponding increase of P_{H2} redirect HA towards EtOH formation. EtOH was first detected five days after the shift (on day 35) and followed an accumulation trend, reaching 80 mM C on day 230 under the different conditions tested (Table 1).

dCO_2 transitions from higher to lower range periods positively influenced EtOH selectivity. An EtOH production increase was observed from day 30, when dCO_2 range was lowered from 1000 to 1250 to 200–800 mg L^{-1}, and from day 85, when the dCO_2 range was further narrowed to 100–300 mg L^{-1}, and on day 147 when dCO_2 was set between 100 and 150 mg L^{-1}. Overall, the best conditions for EtOH production in R-A were: dCO_2 controlled at 100–300 mg L^{-1}, pH between 4.5 and 4.8, and maximum P of 1.8 bar, resulting in the highest production rate of 4.19 g m^{-2} d^{-1} between days 92 and 95. The dCO_2 range 100–300 mg L^{-1} was high enough to sustain HA production for further conversion to EtOH via solventogenesis, while the dCO_2 range 100–150 mg L^{-1} (on days 147–172) resulted in a decrease of HA concentration. This suggests that dCO_2 should not be lowered below a threshold to support concomitant HA and EtOH formation. Below this threshold, CO_2 limitation occurred, impairing HA maintenance resulting in a reduced EtOH formation.

Following the procedure conducted in R-A, the R-B system was operated under similar conditions to reproduce these findings. Operation of reactor R-B began under conditions promoting HA production (dCO_2 = 1000–1250 mg L^{-1}, pH = 4.8–5.0 and P = 1.6 bar), resulting in HA accumulation up to 224 mM C between day 3 and 27, with a mean production rate of 23.42 g m^{-2} d^{-1}. This performance represented a substantial improvement compared to the initial period of R-A (8.13 g m^{-2} d^{-1}). Afterwards, the best conditions for EtOH production identified in R-A (dCO_2 = 100–300 mg L^{-1}, pH = 4.5–4.8, and P = 1.8 bar) were applied to R-B. Under these conditions, R-B achieved an EtOH production rate of 14.80 g m^{-2} d^{-1} on days 27 to 35, reaching a final titre of 91 mM C (2.1 g L^{-1}) and 55% product selectivity. The higher EtOH production rates obtained in R-B were probably linked to the use of an already acclimated inoculum, and to the fine-tuned conditions timely applied based on the experience gained with R-A.

So far, literature focused on EtOH production (Table S1) is limited and mostly oriented to optimize operation conditions such as pH and CO_2, and evaluate different reactor designs (tubular, H-type, flat-plate, multiple chambered) or CO_2 feeding strategies (continuous sparging, GDE, and supply on demand). This study applied a stackable flat-plate reactor, a convenient configuration to process scale-up and precise control policies for pH, CO_2 and P, favouring the different stages of the process and allowing to obtain the highest EtOH production rate to date (14.80 g m^{-2} L^{-1}). The influence of such operational parameters on EtOH production rate was established in previous studies. For instance, Romans-Casas et al. [12] reported that pressure accumulation (up to 3 bar) in H-type MES cells resulted in an EtOH production rate of 10.95 g m^{-2} L^{-1}. Although glass H-type reactor holds a scalability limitation, this study revealed the significant contribution of maintaining a high H_2 partial pressure in the system to favour solventogenesis. Srikanth et al. [10] accumulated up to 15 g L^{-1} EtOH in GDE-based MES cells, although achieving a lower selectivity (45%) than in the present work (54.8%) mainly due to the onset of chain elongation pathways. The GDE allowed to maintain a dCO_2 of 400 mg L^{-1} [10], while this study demonstrate that lower dCO_2 is required for selective EtOH production. The controlled condition for CO_2, pH and P added to direct current supply (j = 11.25 A m^{-2}) resulted in a total coulombic efficiency of 55.2% (E_{cell} = 3.77 ± 0.37 V). Overall, the strict parameter control applied to this study allowed to obtain higher EtOH concentration (3.9 vs 0.46 g L^{-1}), production rate (14.80 vs 5.69 g m^{-2} L^{-1}), and total CE (55.2 vs 24.7%) than a previous study in bench-scale MES platform [13].

3.2. Pattern analysis of the MES production stages

The MES process is extremely sensitive to operational conditions, so that its optimization requires timely analyses of key parameters. Conventional product quantification methods, such as GC or HPLC, are time-consuming and provide only discrete measurements. Consequently, these methods yield limited information about system dynamics. Leveraging real-time data is crucial to understand the process behaviour through pattern discovery, particularly when evaluating productivities over specific operational periods.

In the pattern recognition approach, following the completion of MES cell operation, process data were visualized to identify periods exhibiting stable trends in performance variables (EtOH and HA production rates). This analysis resulted in sixteen periods indicated as "stages" (Fig. 3). The corresponding datasets of O.V. signals were subsequently analysed individually to obtain insights into the process dynamics. Table 2 lists for each stage, the corresponding time interval, the set conditions of the controlled variables, and EtOH and HA productivities. The production stages were grouped in three distinct production scenarios: "EtOH Selective" for the stages where ethanol was the main product, "Simultaneous EtOH and HA Production" where both compounds were produced, and "HA Selective" where acetic acid was

Table 2
Selected stages grouped by production scenario, reactor, set conditions of controlled variables and production rates of EtOH and HA. Values with "-"means negligible production rate, while negative values are referred to consumption periods.

Production scenario	Reactor	Stage	Period	Controlled variable			Productivity	
				dCO_2	pH	P	EtOH	HA
			d	mg L^{-1}	–	bar	g m^{-2} d^{-1}	
EtOH Selective	R-B	XIII	27–35	100–300	4.5–4.8	1.8	14.80	−4.34
	R-A	VI	92–95				4.19	−1.74
		VIII	147–172	100–150			2.09	−1.88
		IX	172–191	100–300			0.78	–
Simultaneous EtOH and HA Production	R-B	XI	8–16	1000–1250	4.8–5.0	1.6	5.47	24.67
		XIV	35–52	100–300	4.5–4.8	1.8	5.31	2.23
	R-A	V	86–95				2.62	6.82
		VII	112–128				1.46	3.08
	R-B	XV	55–85				1.04	8.03
	R-A	II	30–38	200–800		1.6	1.01	14.20
		X	193–231	100–300		1.8	0.95	1.69
	R-B	XVI	94–111				0.76	11.37
HA Selective	R-B	XII	16–27	1000–1250	4.8–5.0	1.6	−0.69	22.16
	R-A	IV	70–79	200–800	4.5–4.8	1.8	−1.67	12.39
		I	6–30	1000–1250	4.8–5.0	1.6	–	8.13
		III	49–63	200–800	4.5–4.8		–	6.47

the main product.

The EtOH Selective group is formed by four different stages, which presented EtOH as the single product formed at a rate ranging from 0.78 up to 14.80 g m^{-2} d^{-1}. These results are in line with the literature, where solventogenesis has been reported in production rates ranging from 0.31 to 10.95 g m^{-2} d^{-1} in flat plate reactors [10–12,27]. In these four stages, automated control allowed to maintain dCO_2 between 100 and 300 mg L^{-1}, pH between 4.5 and 4.8 and a pressure of 1.8 bar to promote EtOH formation. Controlled conditions, together with the previous adaptation of the inoculum that achieved fast accumulation of HA, favoured higher EtOH production rates.

The Simultaneous EtOH and HA production was the most common during the experiments. This scenario was observed with almost every control strategy (Table 1), with dCO_2 in the range from 100 to 1250 mg

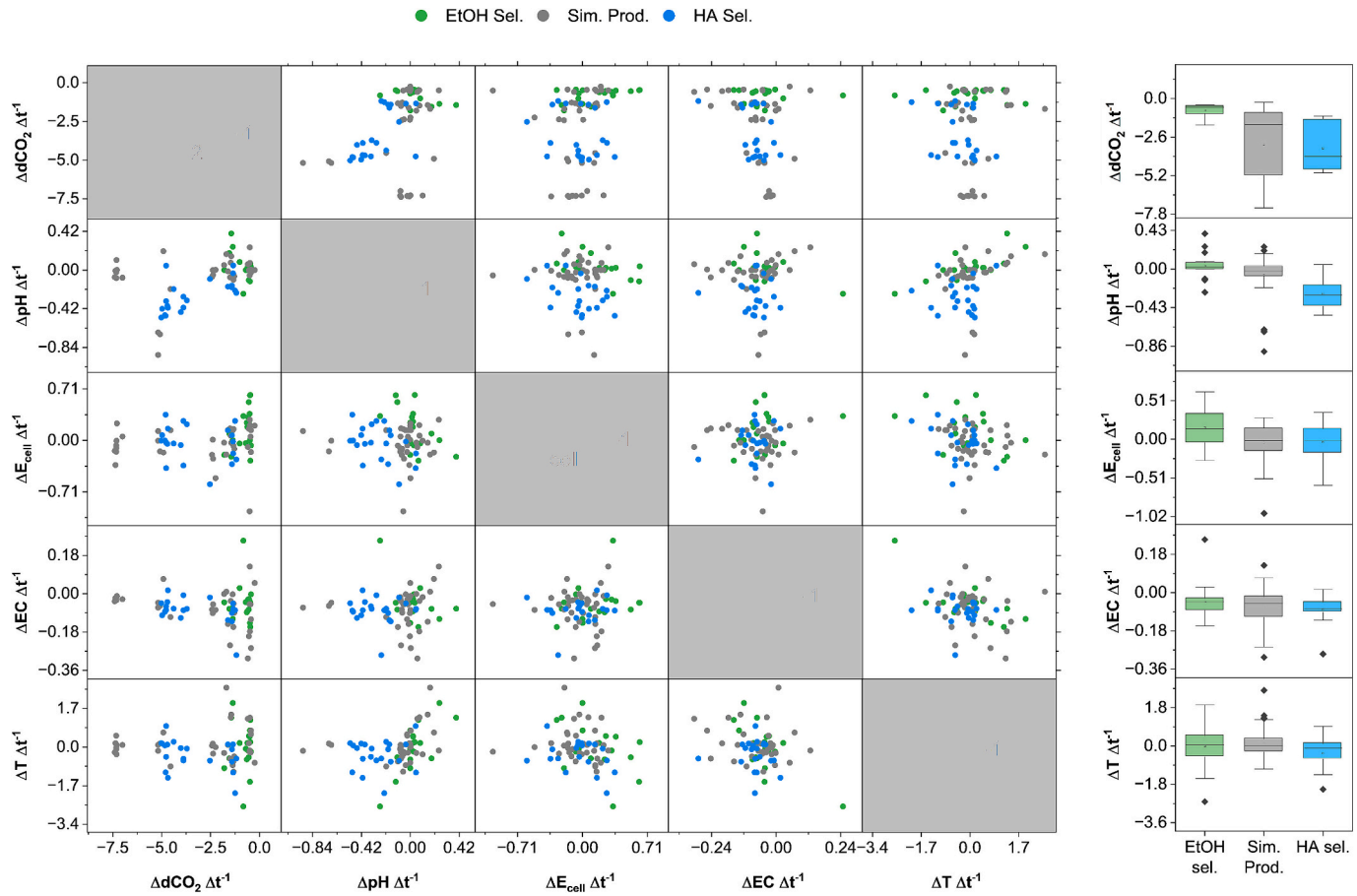

Fig. 4. Relationship between operational variables (ΔdCO_2 Δt^{-1}, ΔpH Δt^{-1}, ΔE_{cell} Δt^{-1}, ΔEC Δt^{-1}, and ΔT Δt^{-1}) grouped by production scenario; EtOH selective (green), HA selective (blue), simultaneous production (grey). Each point in the plot represents a local slope of the variable within the respective production scenario related in Table 2. Box plots distribution is shown in the diagonal of the matrix.

L^{-1}, pH from 4.5 to 5.0 and pressures of 1.6 and 1.8 bar. Even though there were conditions supposed to promote solventogenesis, HA production was not completely hampered. This was probably because of the mixed culture used to inoculate MES cells, which included acetogens active at low pH. The HA promoting scenario occurred at high dCO_2 concentrations (1000–1250 and 200–800 mg L^{-1}) and pH ranging from 4.5 to 5.0, confirming that HA is the main product when dCO_2 is abundant, even at low pH. A minimum pH of 4.5 was set to avoid acid crash in bacterial community, as stated in the literature [28]. Temperature was not controlled but continuously monitored throughout the process, with an average of 24.0 ± 2.7 °C and 23.4 ± 3.1 °C for R-A and R-B, respectively, highlighting the capability of the microbial community to sustain CO_2 reduction at sub-optimal temperature conditions.

During the "EtOH Selective" stages, pH showed increasing trends as a result of HA consumption, except for Stage IX, where the EtOH production rate was low. Instead, in the "HA Selective" and "Simultaneous EtOH and HA production" scenarios, pH signals had continuous decreasing trends, only changed by the spike injections of NaOH to stay among the set limits.

Although grouping and visual analysis of the controlled variables signal provides qualitative information on a certain scenario, limited quantitative insights can be extracted. A quantitative analysis of each dynamic variable was then conducted to expand comprehension of the process. To illustrate the correlation between variables, several local slopes of standardized O.V. were extracted within every stage to compare production scenarios (Table S2). Local slopes were selected avoiding CO_2 injections or acid/base dosing that alter the actual dynamics of the variable. Those slopes are representation of the increasing or decreasing rates within the same predefined time window for all O.V. Fig. 4 shows the scatter matrix plot of each O.V. slopes and the box distribution (right graphs), grouped by the production scenario.

The analysis revealed that EtOH selective stages presented less negative $\Delta dCO_2\ \Delta t^{-1}$ values, indicating slower CO_2 consumption, confirming that EtOH was produced by HA conversion, rather than directly from CO_2. On the contrary, the HA selective scenario was characterized by more negative $\Delta dCO_2\ \Delta t^{-1}$ because acetogenesis results in a rapid CO_2 consumption. From a thermodynamic perspective, hydrogenotrophic acetogenesis is more advantageous than acetate reduction to ethanol using H_2, with energy values of −94.96 kJ mol^{-1} compared to −10.50 kJ mol^{-1}, respectively. Thus, a greater CO_2 consumption was observed during HA selective stages. [29] The most negative $\Delta dCO_2\ \Delta t^{-1}$ values were obtained under the Simultaneous EtOH and HA production scenario. This scenario suggested high CO_2 consumption due to HA formation and its subsequent reduction to EtOH, but at the same time allowing HA accumulation. However, simultaneous production of HA and EtOH presented a wide distribution of $\Delta dCO_2\ \Delta t^{-1}$ values since in those stages both processes were taking place but none of them prevailed. Regarding pH, the EtOH selective stages were characterized by a positive $\Delta pH\ \Delta t^{-1}$ as the pH increased when HA was consumed to produce EtOH. This dynamic was caused by HA conversion to EtOH, a detoxifying mechanism to avoid acid crash in acetogenic bacteria [30]. In the other two scenarios, $\Delta pH\ \Delta t^{-1}$ was negative (pH decreases), due to HA production. Several MES studies with significant EtOH formation evidenced a pH decreasing trend, indicating acetic acid accumulation as a consequence of CO_2 reduction [11,12,31,32]. Blasco-Gomez et al. [11] reported that replicable cycles of acetogenesis and solventogenesis occur when intermittently supplying 800 mg L^{-1} CO_2 to MES cells. Therefore, the wide distribution of pH dynamics in R-A and R-B was probably associated with periods of either EtOH or HA prevalent production.

Spearman correlation coefficients were computed for O.V. dynamics ($\Delta var\ \Delta t^{-1}$) within the production scenarios (correlation results are summarized in Tables S3-S5), providing relationships between operational variables. For instance, during the EtOH selective stages, a positive $\Delta pH\ \Delta t^{-1}$ correlated with a positive $\Delta T\ \Delta t^{-1}$ ($r' = 0.653$, *p-value* = 0.003), and with a negative $\Delta E_{cell}\ \Delta t^{-1}$ ($r' = -0.492$, *p-value* = 0.038). The external daily temperature fluctuation during long term experiments affected variables such as pH. In fact, a T increase resulted in lower CO_2 solubility, which is reflected in a pH increase. Hence, pH dynamics could be an indicator of selective organics production, but T should be controlled to avoid pH signal perturbations. On the other hand, the decreasing trend of E_{cell} was reflecting the increase of EC of the medium due to HA production and the consequent NaOH addition.

In HA selective stages, $\Delta pH\ \Delta t^{-1}$ correlated positively with $\Delta dCO_2\ \Delta t^{-1}$ ($r' = 0.695$, *p-value* = 4.73exp-4). This indicates that fast dCO_2 consumption correlates to sharp pH decreases due to HA accumulation. Additionally, in HA production stages, $\Delta dCO_2\ \Delta t^{-1}$ was negatively correlated to $\Delta T\ \Delta t^{-1}$ (r' -0.436, *p-value* = 0.048). This behaviour can be related to gas solubility and microbial kinetics dependence on temperature. During the simultaneous EtOH and HA production, only $\Delta pH\ \Delta t^{-1}$ (and not $\Delta dCO_2\ \Delta t^{-1}$) significantly correlated with $\Delta T\ \Delta t^{-1}$ ($r' = 0.720$, *p-value* = 0.008). This was also observed during the EtOH selective stages, in which pH measurements were influenced by T fluctuation.

3.3. Unsupervised phases identification

To better understand the system's behaviour beyond the predefined productivity stages, an unsupervised clustering approach was applied to the operational variables. Differently from the supervised analysis, this approach aimed at uncovering data-driven temporal patterns in O.V. that might reveal shifts in production scenarios without inputting the P.V. The output of this analysis were "phases" obtained from exclusively standardized O.V. dataset.

The SCFCM algorithm allowed the identification of nine different phases for R-A (*a* to *i*) and five for R-B (*j* to *n*) without needing quantitative production data. A timeline comparison between the identified phases and the previously selected productivity stages is shown in Fig. 5. Overall, the identified phases were in line with the stages, confirming that the algorithm can be trained to detect production scenarios based only on operational parameters.

The time boundaries between phases were not strictly consecutive, as bioelectrochemical systems often experience transition periods between stable phases. These transitions reflect the internal dynamics of the process, during which equilibrium is gradually reestablished and a new state of correlation among the operational variables emerges. However, stages and phases coincided when operational changes were imposed (control regimes) or even when they spontaneously occurred. These alignments mean that the phases can be directly related to production scenarios. Slight temporal differences between phases and stages may be attributed to different sampling frequency (i.e., operational variables signals were collected every minute, while organics were analysed every 2 to 3 days).

Overall, the algorithm identified nine phases in R-A, each characterized by distinct patterns of correlation among the O.V. The Phase *a,* (days 0 to 7) represents the process start up, when pH was adjusted to the set range and EC found an equilibrium, with low organics production. After the starting period, Phase *b* can be aligned to Stage I despite the clustering algorithm identified the starting time slightly later. Phase *b* corresponds to an acetogenesis selective stage, confirming the successful detection of variables that can be related to HA production by the unsupervised algorithm. Other HA selective phases were Phase *d,* which was closely related to Stage IV, and Phase *i* which was synchronized to Stage X. EtOH selective phases were identified in Phases *g* and *h*, related to Stages VIII and IX. Phases *c* and *e* overlapped two stages (II-III, and V-VI, respectively) because the dCO_2 and pH signals remained within the same range, while EC had a decreasing trend. Such signals provided stable data that induced SCFCM to classify them as a single phase, even though different productivities were obtained within these periods. Phase *f* was shorter than Stage VII, but they can be associated because, on days 115 to 128, most operational variables presented the same control regime. Nevertheless, operational deviations in dCO_2 induced the SCFCM algorithm to classify it as a short phase. This highlights the importance of integrating expert process knowledge into emerging data-

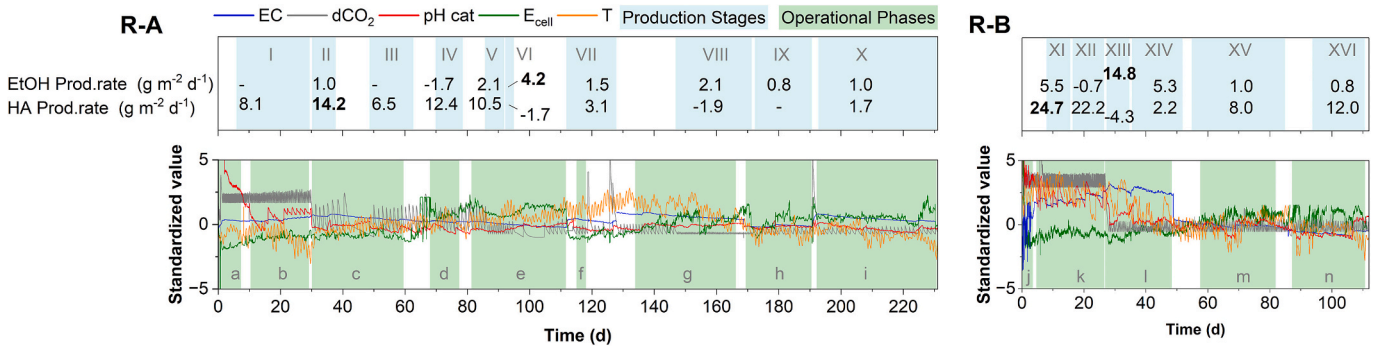

Fig. 5. Comparison between production stages (blue periods, labelled I to XVI) defined by expert knowledge based on productivity of EtOH and HA, and phases (green periods, labelled a to n) obtained with the Sequenced Constrained Fuzzy C-means (SCFCM) algorithm based only on operational variables (EC, dCO_2, pH, E_{cell}, and T). Production rates of EtOH and HA are shown along with stages, where the highest values are in bold. Line plots are standardized values of each variable signal, inputted to SCFCM algorithm.

driven methods, ensuring more reliable models that represent the system dynamics and understanding their limitations when raw experimental data is utilized [33].

Phases identification in R-B was similar to R-A. The Phase *j* referred to a starting up period, and the following Phase *k* represented a pseudo-stationary acetogenic period enclosing Stages XI and XII. The algorithm successfully detected the shift from Phase *k* to *l* on day 27, when the operational conditions were switched to promote solventogenesis. From day 27, Phase *l* enclosed production Stages XIII and XIV, corresponding to solventogenesis with decreases in EC and E_{cell} marked by clean signals. Despite the lower EtOH production rate obtained from day 35 to 52 in Stage XIV, the unsupervised SCFCM interpreted a single operation condition from day 27 up to day 48. The lower number of phases identified compared to the production stages may be favourable for the development of a simpler MES model, as stated by Lu et al. [34]. Such simpler model could allow to further refine the control strategies leading to a more accurate phase partition between EtOH and HA production scenarios. Small changes in productivity could be refined through more frequent sampling of the system in such critical stages and/or incorporating additional operational variables that provide additional information on process evolution. In R-B, the identified phases were longer than in R-A due to the higher process stability and the longer periods with each operation control regime. Nevertheless, the algorithm identified different phases (i.e., *l* to *n*), implying its ability to recognize the different correlations between operational variables under the same controlled conditions. These phases were different due to the contribution of monitored variables such as EC and E_{cell} that were not controlled but evolved according to process performance and provide information about process dynamics [32].

3.4. Operational phases statistical model

Once the phases are synchronized with production stages, each phase can be individually modelled to understand the variables affecting production. One advantage of the unsupervised approach is the low computational requirements to define the phases based only on process

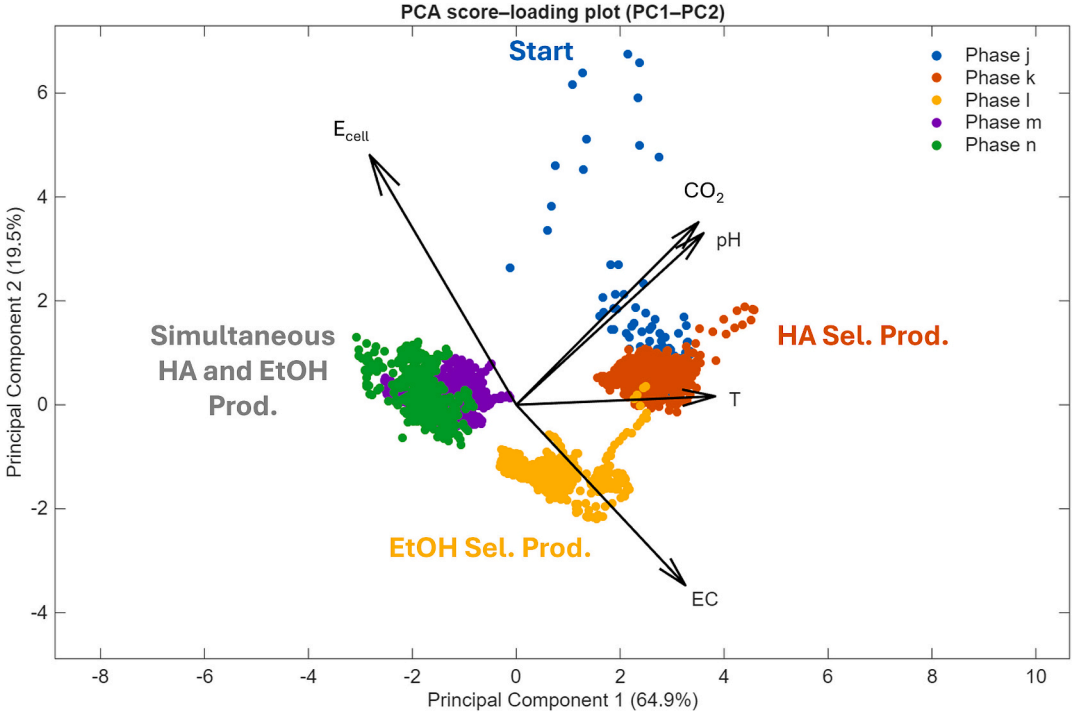

Fig. 6. Scatter plot of the O.V. data from the whole Reactor-B run, with their respective loadings, projected in the first two principal components. Distinct clusters (j–n) reflect the chronological phases identified by SCFCM. Loading vectors are scaled for visualization and do not represent their absolute magnitude.

data, which is immediately available through the SCADA module connected to the BES platform.

As R-B presented stable performance and better data quality, it was chosen as the reference batch to develop PCA. First, PCA was carried out taking the experimental run as a unique phase to observe the variability of O.V. over time. Fig. 6 shows the scatter plot of R-B data projected onto the first two principal components (PC1 and PC2) space and the O.V. loadings. The formation of distinct clusters (labelled *j* to *n*), indicate the O.V. transitioned through different correlation patterns, referred as phases. The clear separation of these clusters highlights that each phase represents a unique operational state. Additionally, the spatial separation between phases in Fig. 6 underscores the need for individual analysis to capture specific dynamics of the O.V. at each stage. Phase transitions were a consequence of the O.V. dynamics, and the loadings orientation indicate the probable mechanisms for each operational state. Separated clusters in PC1-PC2 space validated the SCFCM as unsupervised clustering method for O.V. dataset, as SCFCM conserved the temporal order of data and revealed the process evolution throughout the transition of the different operational phases (Fig. 6) [22].

To explore the internal variability of each phase, PCA was applied separately to the O.V. data corresponding to each phase. This approach revealed the dominant sources of variability and the variable interactions that define the distinctive patterns of each phase. Fig. 7 summarizes PCA results for each phase, showing the variance explained by each principal component and the accumulative variance. Below, the loading plots illustrate the contribution of dCO_2, pH, EC, T, and E_{cell} in the projected space (Principal Component 1 and 2). Phase *k* was taken for HA selective production, *l* was considered for EtOH selective production, and *m* was selected as associated with simultaneous production. Tables S5-S7 summarizes the loadings in principal components for the Phases *k*, *l* and *m*. Interestingly, most of the variability in the three phases can be explained by PC1, which represents 80–86% of the total data variance. Therefore, information contained in PC1 suggests well-defined patterns in the relationships among O.V. during each phase.

The PCA results reveal that each phase can be explained by two or three principal components, which is the objective of simplifying multivariate process data into a reduced dimension [35]. Also, the PCA captured how the reactor responded when different control regimes were applied. The loadings plot for the HA selective production phase indicated that PC1 was primarily defined by dCO_2 patterns (loading = 0.62), with moderate positive contributions of T, pH, and EC (loadings 0.47, 0.45 and 0.31, respectively). The similar contribution of these variables indicated a direct correlation among them during such phase. Operationally, HA production is carbon-driven ($dCO_2 > 1000$ mg L^{-1}) and evidence a positive correlation between EC and pH in PC1, because relatively high pH was controlled (pH > 4.8) by NaOH addition, further increasing EC. In contrast, E_{cell} strongly influenced PC2 and was decoupled from PC1, indicating an electrochemical independent variability pattern from the rest of variables (dCO_2, pH, EC, and T) related to the electrolyte chemical composition.

In the EtOH selective production Phase *l*, the EC was the variable that contributed the most to variability (loading 0.81), as a consequence of ion accumulation regime during the previous HA synthesis and NaOH dosing. This EtOH production period was initially characterized by a conductive electrolyte, while dCO_2 was under lower range (100–300 mg L^{-1}) and the availability of HA was decreasing. Afterwards, EC decreased due to biological HA consumption and ion redistribution between cathodic and anodic chambers. EC negatively correlated to E_{cell}, which increased due to the increasing ohmic resistance of the electrolyte. PCA loading plots (Fig. 7-b) for Phase *l* showed that pH did not correlate to EC in PC1 in the same way as in the other two phases (*k* and *m*). This is in line to findings of section 3.2, where the spearman correlation between $\Delta pH\ \Delta t^{-1}$ and $\Delta EC\ \Delta t^{-1}$ was different only for EtOH production scenario because pH increases while EC decreases continuously.

In the simultaneous EtOH and HA production Phase *m*, T appeared with the most variability in both PC1 and PC2. T reflected daily and seasonal change during the experiment, as it was not controlled,

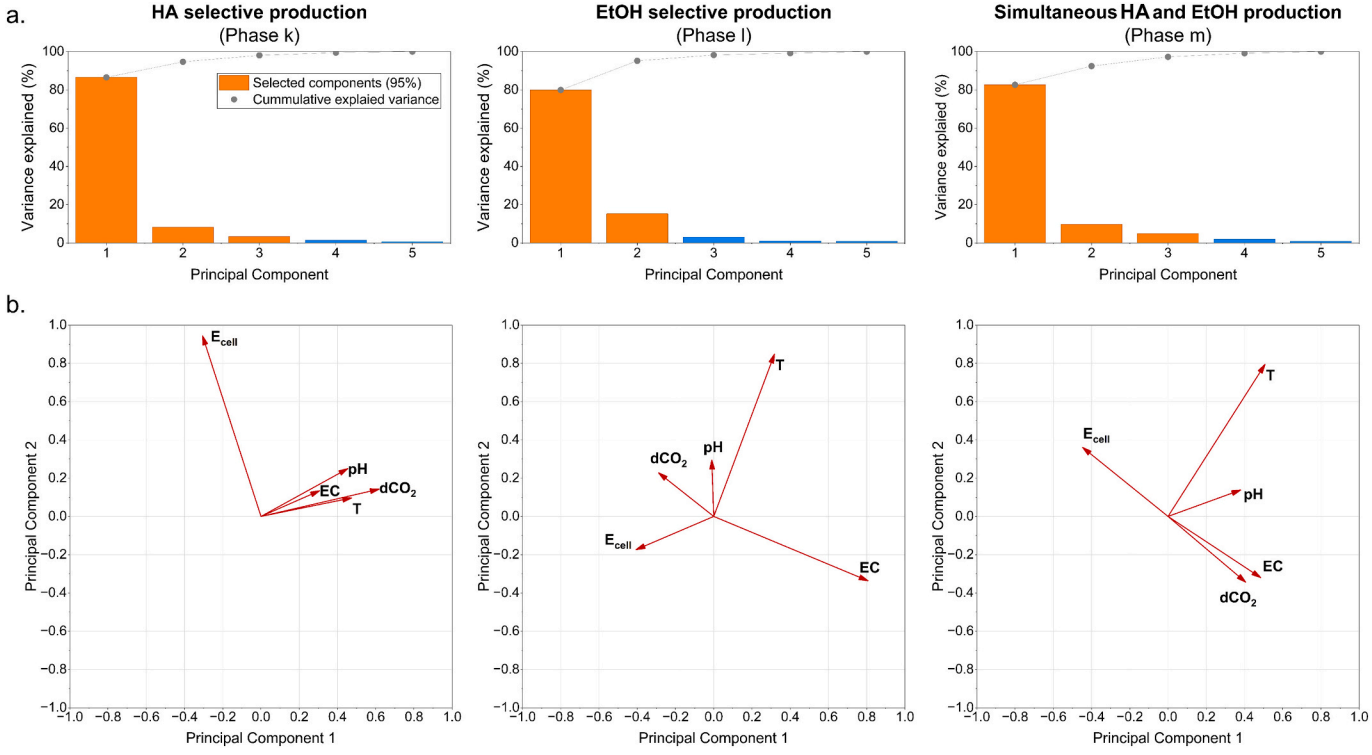

Fig. 7. (a) Variance explained of principal components and cumulative variance. Orange bars highlight the components retained for interpretation, which represent 95% of phase variance. (b) Variable loadings in the first two principal components that indicate critical operational variables associated with EtOH Selective, HA Selective, and Simultaneous Production in MES.

generating structured noise, rather than providing insights on process response. In fact, temperature not only affects the microbial kinetics, but also CO_2 and H_2 solubility that directly impact on process performance. For instance, syngas fermentation and CO_2 bio-electrorecycling controlled at 25 °C was proposed by literature [11,28] to promote solventogenesis by acetogenic cultures. An effective T control would simplify the analysis of the remaining O.V. by eliminating their thermal dependence and providing suitable environmental conditions for solventogenesis. Even though, EC, dCO_2, and pH accompanied the variance of PC1, which indicated the concentration of ions and CO_2 were also dependent on T in culture media.

In Phase *m*, EtOH selectivity decreased probably due to ion depletion, as indicated by the decreasing EC signal and the increasing E_{cell}. Rovira-Alsina et al. [29] demonstrated process recovery after partial media replacement to reintegrate nutrients in thermophilic acetogenesis. This strategy could also be applied to refresh essential nutrients for solventogenesis but affect process downstream.

4. Implications

The identification of production stages and their association with operational phases is essential, as real-time measurement of HA and EtOH concentrations is technically challenging and costly. Optimizing production therefore relies on recognizing characteristic patterns in readily available operational variables, enabling timely corrective actions. Effective application of data-driven methods in MES requires process expertise to interpret variable dynamics and prioritize critical productivity factors [36]. Data quality is crucial: sensors, transmitters, and PLCs must be calibrated and maintained to provide representative measurements, while structured workflows and preprocessing ensure reliable data management from SCADA to monitoring, fault diagnosis, and predictive tools [37]. Visualization tools, such as statistical process charts, facilitate understanding and operational decisions even without offline product measurements [38].

Data-rich experimentation, as employed here, provides a foundation for applying these methods to other MES. High-frequency datasets can optimize production of compounds such as methane, H_2, or butyric acid, using physicochemical (substrate concentration, pH, temperature) and electrochemical (cell voltage, current density) variables. Limitations include batch-to-batch variability, microbial community shifts, and sensor resolution or delays, which may affect pattern recognition and reproducibility. Integrating microbiome information, careful sensor selection, calibration, preprocessing, and expert knowledge with robust data workflows is therefore essential to develop reliable data-driven models and enable effective real-time monitoring and control under challenging conditions.

5. Conclusions

In this study, bench scale MES cells were operated within an automated platform that enabled real-time monitoring and control of key operational variables (dCO_2, pH, pressure, EC, E_{cell} and temperature). Systematic analysis of the collected datasets through pattern discovery within production stages and unsupervised clustering based on operational variables enabled the identification of distinct operational phases and the correlations that govern HA and EtOH product formation.

Selective ethanol production was achieved under controlled conditions of pH 4.5–4.8, dCO_2 100–300 mg L^{-1}, and 1.8 bar, yielding the highest EtOH production rate of 14.80 g m^{-2} d^{-1}, highlighting the need for precise control of these parameters. EtOH productivity correlated with decreasing EC, making this signal a reliable real-time indicator of solventogenic activity. Each operational phase displayed distinct correlations among variables, supporting the adoption of phase-specific monitoring and control strategies to improve system stability and performance. Overall, successful digitalization of MES requires the integration of high-quality, high-frequency data with process expertise, reliable instrumentation, and robust workflows for data management and visualization.

CRediT authorship contribution statement

Jorge A. Albarracin-Arias: Writing – original draft, Visualization, Methodology, Investigation, Data curation, Conceptualization. **Meritxell Romans-Casas:** Writing – review & editing, Supervision, Methodology, Investigation, Conceptualization. **Paolo Dessì:** Writing – review & editing, Supervision, Methodology. **M. Dolors Balaguer:** Writing – review & editing, Supervision, Resources, Methodology, Conceptualization. **Sebastià Puig:** Writing – review & editing, Supervision, Resources, Project administration, Conceptualization.

Declaration of competing interest

The authors declare that they have no known competing financial interests or personal relationships that could have appeared to influence the work reported in this paper.

Acknowledgements

This research was carried out within the project "PANGEA – Process intensificAtioN for bioelectroCO_2 recyclinG into carbon-nEutrAl products), funded by the Spanish Ministry of Innovation and Science (ref. PID2021-126240OB-I00), and the European Union's Horizon Europe research and innovation program under the project "Fuels-C" (Grant No. 10111560). J.A acknowledges funding from the Spanish Ministry of Innovation and Science (PRE2022-101241). P.D. is financially supported by the project RESTART, funded through the "Dipartimenti di Eccellenza 2023-2027" initiative of the Italian Ministry of University and Research. S.P. is a Serra Húnter Fellow (UdG-AG-575) and gratefully acknowledges funding from the AGAUR–ICREA Acadèmia Programme, supported by the Department of Research and Universities of the Government of Catalonia. LEQUIA has been recognized by the Catalan Government (Ref 2021 SGR01352). Open Access funding was provided through the CRUE-CSIC agreement with Elsevier.

Appendix A. Supplementary data

Supplementary data to this article can be found online at https://doi.org/10.1016/j.cej.2026.174960.

Data availability

Data will be made available on request.

References

[1] P. Dessì, L. Rovira-Alsina, C. Sánchez, G.K. Dinesh, W. Tong, P. Chatterjee, M. Tedesco, P. Farràs, H.M.V. Hamelers, S. Puig, Microbial electrosynthesis: towards sustainable biorefineries for production of green chemicals from CO_2 emissions, Biotechnol. Adv. 46 (2021), https://doi.org/10.1016/j.biotechadv.2020.107675.

[2] K. Rabaey, R.A. Rozendal, Microbial electrosynthesis - revisiting the electrical route for microbial production, Nat. Rev. Microbiol. 8 (2010) 706–716, https://doi.org/10.1038/nrmicro2422.

[3] Market Observatory for Energy of the European Commission, Quarterly report On European gas markets Market Observatory for Energy DG Energy, 2024.

[4] X. Christodoulou, S.B. Velasquez-Orta, Microbial electrosynthesis and anaerobic fermentation: an economic evaluation for acetic acid production from CO_2 and CO, Environ. Sci. Technol. 50 (2016) 11234–11242, https://doi.org/10.1021/ACS.EST.6B02101.

[5] Argus Media group, Viewpoint: EU Ethanol Prices Likely to Rise in 2024 | Latest Market News, Biofuels, Market, 2023 https://www.argusmedia.com/en/news-and-insights/latest-market-news/2522646-viewpoint-eu-ethanol-prices-likely-to-rise-in-2024?utm_source=chatgpt.com (accessed August 14, 2025).

[6] M.T. Agler, C.M. Spirito, J.G. Usack, J.J. Werner, L.T. Angenent, Chain elongation with reactor microbiomes: upgrading dilute ethanol to medium-chain carboxylates, Energy Environ. Sci. 5 (2012) 8189–8192, https://doi.org/10.1039/C2EE22101B.

[7] P. Dessì, M. Romans-Casas, E. Perona-Vico, M. Tedesco, H.V.M. Hamelers, L. Bañeras, M. Dolors Balaguer, S. Puig, Membrane-based fermentation enables highly selective caproic acid production from wine lees, Chem. Eng. J. 497 (2024) 154539, https://doi.org/10.1016/J.CEJ.2024.154539.
[8] Á. Fernández-Naveira, M.C. Veiga, C. Kennes, H-B-E (hexanol-butanol-ethanol) fermentation for the production of higher alcohols from syngas/waste gas, J. Chem. Technol. Biotechnol. 92 (2017) 712–731, https://doi.org/10.1002/JCTB.5194.
[9] K.J.J. Steinbusch, H.V.M. Hamelers, C.J.N. Buisman, Alcohol production through volatile fatty acids reduction with hydrogen as electron donor by mixed cultures, Water Res. 42 (2008) 4059–4066, https://doi.org/10.1016/J.WATRES.2008.05.032.
[10] S. Srikanth, D. Singh, K. Vanbroekhoven, D. Pant, M. Kumar, S.K. Puri, S.S. V. Ramakumar, Electro-biocatalytic conversion of carbon dioxide to alcohols using gas diffusion electrode, Bioresour. Technol. 265 (2018) 45–51, https://doi.org/10.1016/J.BIORTECH.2018.02.058.
[11] R. Blasco-Gómez, S. Ramió-Pujol, L. Bañeras, J. Colprim, M.D. Balaguer, S. Puig, Unravelling the factors that influence the bio-electrorecycling of carbon dioxide towards biofuels, Green Chem. 21 (2019) 684–691, https://doi.org/10.1039/C8GC03417F.
[12] M. Romans-Casas, E. Perona-Vico, P. Dessì, L. Bañeras, M.D. Balaguer, S. Puig, Boosting ethanol production rates from carbon dioxide in MES cells under optimal solventogenic conditions, Sci. Total Environ. 856 (2023) 159124, https://doi.org/10.1016/j.scitotenv.2022.159124.
[13] M. Romans Casas, Bio-Electro CO_2 Recycling into Added Value Compounds: Insights, Routes, Strategies and Performance Improvements, Universitat de Girona, 2025 https://www.tdx.cat/handle/10803/693340 (accessed August 4, 2025).
[14] J. Camacho, J. Picó, A. Ferrer, Multi-phase analysis framework for handling batch process data, J. Chemom. (2008) 632–643, https://doi.org/10.1002/cem.1151. John Wiley and Sons Ltd.
[15] L.A. Briceno-Mena, M. Nnadili, M.G. Benton, J.A. Romagnoli, Data mining and knowledge discovery in chemical processes: effect of alternative processing techniques, Data-Centric Engineering 3 (2022) e18, https://doi.org/10.1017/DCE.2022.21.
[16] S. Vlassides, J.G. Ferrier, D.E. Block, Using historical data for bioprocess optimization: modeling wine characteristics using artificial neural networks and archived process information, Biotechnol. Bioeng, B. Bioeng 73 (2001), https://doi.org/10.1002/1097-0290.
[17] H. Le, S. Kabbur, L. Pollastrini, Z. Sun, K. Mills, K. Johnson, G. Karypis, W.-S. Hu, Multivariate analysis of cell culture bioprocess data—lactate consumption as process indicator, J. Biotechnol. 162 (2012) 210–223, https://doi.org/10.1016/j.jbiotec.2012.08.021.
[18] C. Li, D. Guo, Y. Dang, D. Sun, P. Li, Application of artificial intelligence-based methods in bioelectrochemical systems: recent progress and future perspectives, J. Environ. Manag. 344 (2023) 118502, https://doi.org/10.1016/j.jenvman.2023.118502.
[19] S. Gadkari, Application of Artificial Intelligence Methods for the Optimization and Control of Bioelectrochemical Systems, Elsevier Inc., 2022, https://doi.org/10.1016/B978-0-323-90765-1.00023-X.
[20] L. Rovira-Alsina, M. Dolors Balaguer, S. Puig, Transition roadmap for thermophilic carbon dioxide microbial electrosynthesis: testing with real exhaust gases and operational control for a scalable design, Bioresour. Technol. 365 (2022) 128161, https://doi.org/10.1016/J.BIORTECH.2022.128161.
[21] OriginLab Corporation, OriginPro, (n.d.).
[22] L. Luo, S. Bao, J. Mao, D. Tang, Z. Gao, Fuzzy phase partition and hybrid modeling based quality prediction and process monitoring methods for multiphase batch processes, Ind. Eng. Chem. Res. 55 (2016) 4045–4058, https://doi.org/10.1021/acs.iecr.5b04252.
[23] L. Luo, S. Bao, J. Mao, D. Tang, Phase partition and phase-based process monitoring methods for multiphase batch processes with uneven durations, Ind. Eng. Chem. Res. 55 (2016) 2035–2048, https://doi.org/10.1021/acs.iecr.5b03993.
[24] The MathWorks Inc, Matlab, 2025 https://www.mathworks.com (accessed September 2, 2025).
[25] P. Nomikos, Statistical Process Control of Batch Processes, McMaster University, 1995.
[26] L. Chiang, B. Lu, I. Castillo, Big data analytics in chemical engineering, Annu. Rev. Chem. Biomol. Eng. 8 (2017) 63–85, https://doi.org/10.1146/ANNUREV-CHEMBIOENG-060816-101555.
[27] S. Srikanth, M. Kumar, D. Singh, M.P. Singh, S.K. Puri, S.S.V. Ramakumar, Long-term operation of electro-biocatalytic reactor for carbon dioxide transformation into organic molecules, Bioresour. Technol. 265 (2018) 66–74, https://doi.org/10.1016/J.BIORTECH.2017.12.075.
[28] S. Ramió-Pujol, R. Ganigué, L. Bañeras, J. Colprim, Incubation at 25°C prevents acid crash and enhances alcohol production in Clostridium carboxidivorans P7, Bioresour. Technol. 192 (2015) 296–303, https://doi.org/10.1016/J.BIORTECH.2015.05.077.
[29] L. Rovira-Alsina, M. Romans-Casas, M.D. Balaguer, S. Puig, Thermodynamic approach to foresee experimental CO_2 reduction to organic compounds, Bioresour. Technol. 354 (2022), https://doi.org/10.1016/j.biortech.2022.127181.
[30] S.R. Pujol, Insights into Key Parameters for Bio-Alcohol Production in Syngas Fermentation Using Model Carboxydotrophic bacteria, Universitat de Girona, 2016. http://hdl.handle.net/10803/388041.
[31] S. Srikanth, M. Kumar, D. Singh, M.P. Singh, S.K. Puri, S.S.V. Ramakumar, Long-term operation of electro-biocatalytic reactor for carbon dioxide transformation into organic molecules, Bioresour. Technol. 265 (2018) 66–74, https://doi.org/10.1016/J.BIORTECH.2017.12.075.
[32] I. Vassilev, P.A. Hernandez, P. Batlle-Vilanova, S. Freguia, J.O. Krömer, J. Keller, P. Ledezma, B. Virdis, Microbial electrosynthesis of isobutyric, butyric, caproic acids, and corresponding alcohols from carbon dioxide, ACS Sustain. Chem. Eng. 6 (2018) 8485–8493, https://doi.org/10.1021/ACSSUSCHEMENG.8B00739/SUPPL_FILE/SC8B00739_SI_002.XLSX.
[33] M.C. Thomas, W. Zhu, J.A. Romagnoli, Data mining and clustering in chemical process databases for monitoring and knowledge discovery, J. Process Control 67 (2018) 160–175, https://doi.org/10.1016/J.JPROCONT.2017.02.006.
[34] N. Lu, F. Gao, F. Wang, Sub-PCA modeling and on-line monitoring strategy for batch processes, AICHE J. 50 (2004) 255–259, https://doi.org/10.1002/aic.10024.
[35] Z. Ge, Z. Song, Zhiqiang Ge, Zhihuan Song, Multivariate Statistical Process Control. Process Monitoring Methods and Applications, Springer, London, 2013.
[36] José A. Romagnoli, Luis Briceño-Mena, Vidhyadhar Manee, AI in Chemical Engineering: Unlocking the Power within Data, CRC Press, Boca Raton, 2025.
[37] M.R. Dobbelaere, P.P. Plehiers, R. Van de Vijver, C.V. Stevens, K.M. Van Geem, Machine learning in chemical engineering: strengths, weaknesses, opportunities, and threats, Engineering 7 (2021) 1201–1211, https://doi.org/10.1016/J.ENG.2021.03.019.
[38] P. Nomikos, J.F. MacGregor, Multivariate SPC charts for monitoring batch processes, Technometrics 37 (1995) 41–59, https://doi.org/10.1080/00401706.1995.10485888.